JOURNAL OF MATERIALS SCIENCE 29 (1994) 4889–4896

# The morphology and microtexture of $M_7C_3$ carbides in Fe–Cr–C and Fe–Cr–C–Si alloys of near eutectic composition

G. L. F. POWELL, R. A. CARLSON
*CSIRO Division of Manufacturing Technology, P.O. Box 4, Woodville, South Australia 5011*
V. RANDLE
*Department of Materials Engineering, University College of Swansea, Singleton Park, Swansea SA2 BPP, UK*

The microtexture of $M_7C_3$ carbides in undercooled 40 g samples of hyper- and hypo-eutectic Fe–Cr–C alloys was determined by electron back scatter diffraction. In the hyper-eutectic alloy the carbides were monocrystalline, while those in the hypo-eutectic alloy were polycrystalline. While in the former the preferred growth direction of the $M_7C_3$ carbides was [0 0 0 1], in the hypo-eutectic alloy there was a relatively weak texture near [1 0 $\bar{1}$ 1]. There was no evidence for the presence of growth twins in either the $M_7C_3$ carbide rods or in the branching mechanism in the joint between the carbide rods of the hypo-eutectic sample. The morphologies of the $M_7C_3$ carbides resulting from undercooling were used to explain the microstructure of hardfacing Fe–Cr–C weld deposits applied by the manual metal arc process. The effect of silicon additions on the morphology of $M_7C_3$ carbides in Fe–Cr–C–Si alloys is explained in terms of the effect of silicon on undercooling.

## 1. Introduction

High chromium white irons based on the Fe–Cr–C eutectic alloy are used extensively to combat abrasive wear in the minerals processing and related industries [1]. The white irons are utilized both as castings [2] and hardfacing weld deposits [3]. While castings are produced with a eutectic or slightly hypo-eutectic microstructure (primary austenite), hardfacing deposits are usually hyper-eutectic (primary carbide). This is achieved by a multi-layer weld deposit to overcome dilution of the weld layer by the material from the substrate. Hardfacing deposits are subject to tension cracks which often run vertically from the surface of the deposit to the substrate [4]. The fracture surface reveals fractured $(Cr, Fe)_7C_3$ ($M_7C_3$) carbides indicating that the fracture path is through the carbide or through the interface between the carbide and the matrix [5].

Typically, the first layer of a manual metal arc deposit exhibits a substantially eutectic microstructure with a few austenite dendrites at the interface with the steel substrate. Occasionally additional $M_7C_3$ carbides arranged in equilateral triangular patterns are observed, as shown in Fig. 1a [6]. A similar pattern of carbides is sometimes found at the interface between adjacent layers (Fig. 1b) [6]. Second and successive layers are hyper-eutectic with the appearance of the primary carbides dependent upon the geometrical relationship between the plane of section and the axis of the $M_7C_3$ rods. If this plane is parallel to the rod axis the rod morphology of the primary $M_7C_3$ carbides is obvious, whereas if it is perpendicular to the rod axis the primary carbides appear to be equiaxed. The fine eutectic microstructure shown surrounding the equilateral carbide array in Fig. 1a decreases in quantity from the first to the last layer as the quantity of primary carbides increases.

Undercooling is prevalent in surfacing processes. Recently, one of the authors demonstrated that a solid state microstructural change which occurred in the undercooling of alloys could be used to explain the variation in microstructure of plasma sprayed coatings [7]. This paper reports on the morphology and microtexture of the $M_7C_3$ carbide in undercooled Fe–Cr–C alloys and the data applied to explain the development of microstructure in Fe–Cr–C hardfacing weld deposits, particularly in the first and second layers of a multi-layer deposit applied by the manual metal arc process. Finally, the role of silicon in changing the morphology of $M_7C_3$ carbides as the result of undercooling is presented and the results compared with those reported by Atamert and Bhadeshia [8, 9] for the effect of silicon in Fe–Cr–C–Si alloys for consideration as hardfacing alloys.

## 2. Experimental procedure

The hardfacing welds were deposited in four layers using a manual metal arc technique with commercial 4 mm diameter electrodes of the chromium carbide austenitic iron type. This procedure was used to minimize dilution of the top layers from the carbon

0022–2461 

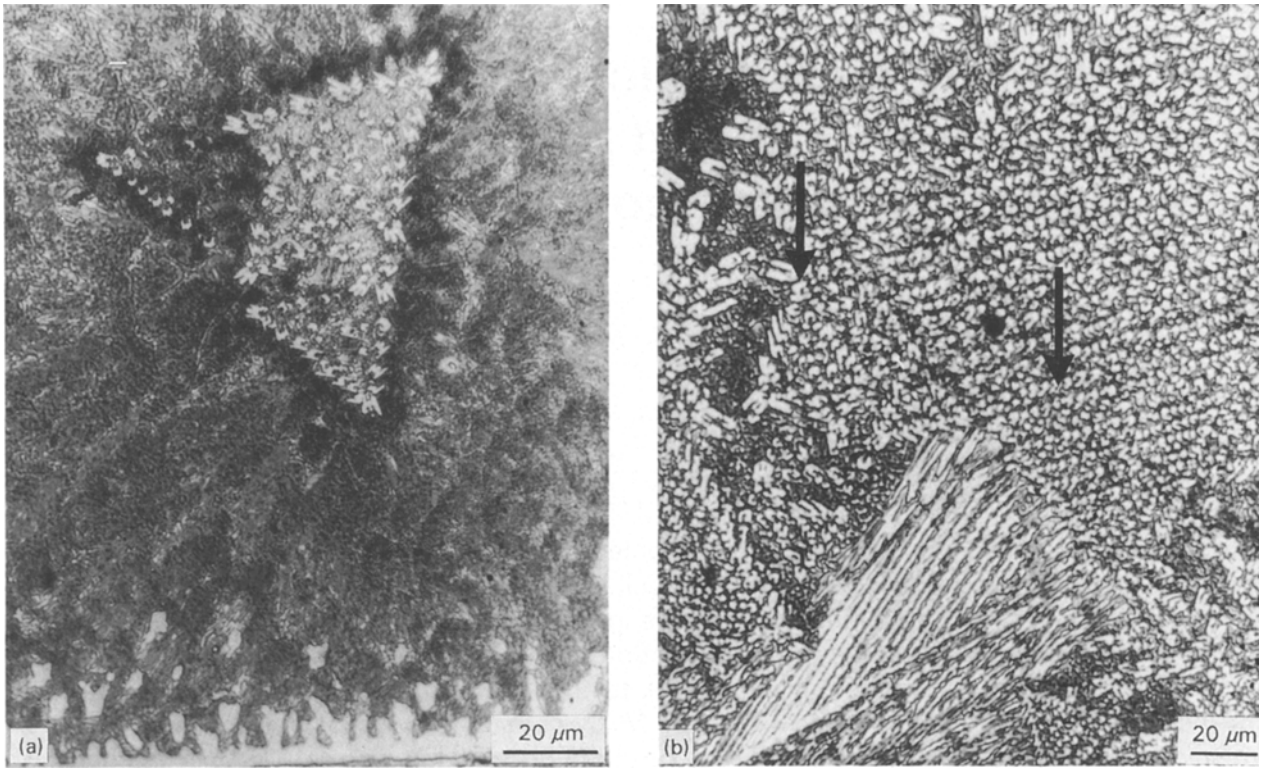


*Figure 1* (a) The microstructure of a perpendicular section through the first layer of a multi-layer Fe–Cr–C alloy hardfacing weld deposit. The substrate carbon manganese steel is at the bottom. Adjacent to the substrate are dendrites of austenite. Note the apparently equiaxed carbides arranged in an equilateral triangular pattern surrounded by a fine unresolvable eutectic of $M_7C_3$ and austenite. (b) The microstructure of $M_7C_3$ carbides in section perpendicular to the substrate at the junction of the first and second layers. Note the arrangement of carbides in equilateral triangular arrays (arrowed). In these arrays the carbide rods were vertical to the plane of section. In the middle bottom of the micrograph the carbide rods are parallel to the plane of polish.

manganese steel substrate. A current of 150 A was used with the d.c. electrode positive. After each weld pass the deposit was allowed to cool to room temperature before the next layer was deposited. Using this procedure the microstructure of the first layer was usually eutectic with succeeding layers hyper-eutectic.

Forty gram melts of Fe–Cr–C alloys were undercooled $> 100$ K with respect to both the liquidus and eutectic temperatures. Final melting was carried out in a radio frequency furnace using a boron-free soda-lime silicate glass slag. The details of the sequence of melting and alloying prior to the final melting have been reported previously [10]. Both hypo-eutectic (Fe–20 wt % Cr–3 wt % C) and hyper-eutectic (Fe–20 wt % Cr–4 wt % C) alloys were undercooled. Individual $M_7C_3$ carbides were examined by electron back scatter diffraction (EBSD) to determine the relative orientation of adjacent carbides [11].

Samples (50 g) of Fe–Cr–C–Si alloys of hyper-eutectic composition with silicon contents up to 7% were melted in a radio frequency induction furnace as described previously [12] and cooled at 0.5 K $s^{-1}$. The compositions were similar to those described by Atamert and Bhadeshia [8, 9]. For optical metallography, the specimens were electrolytically etched in aqueous oxalic acid. Prior to scanning electron microscopy (SEM) for examination of carbide morphology, the samples were deeply etched to remove the matrix.

## 3. Results and discussion

### 3.1. Microtexture of $M_7C_3$ carbides in undercooled hypo- and hyper-eutectic alloys

Fig. 2 shows the boundary between two "grains" in a sample of Fe–Cr–C alloy of hyper-eutectic composition 20 wt % Cr and 4 wt % C undercooled $> 100$ K below the $M_7C_3$ liquidus temperature. The boundary runs from the upper left corner to the bottom right corner in the micrograph. The term grain is used following the terminology in Elliott [13] to indicate growth of a faceted–non-faceted eutectic from a single nucleation centre. Both Laue photographs [10] and EBSD [11] showed that the interconnected carbide within each grain had the same orientation, i.e., it was monocrystalline. In the bottom left-hand corner the carbide rods were parallel to the plane of polish while those in the top right-hand grains were approximately perpendicular to the plane of section. In the grains the [0 0 0 1] direction was parallel to the rod axis indicating that the rods grew in the [0 0 0 1] direction perpendicular to the basal plane. The rods were connected as shown by the arrows in Fig. 2. In the upper right-hand grain the $M_7C_3$ carbide rods formed patterns showing three-fold rotational symmetry. Two common arrays were an equilateral triangle or three carbide rods separated by included angles of approximately 120°. In this sample the thermal data [10] showed that the carbide grew slowly with slow release of latent heat.

The microstructure of a hypo-eutectic 20 wt % Cr

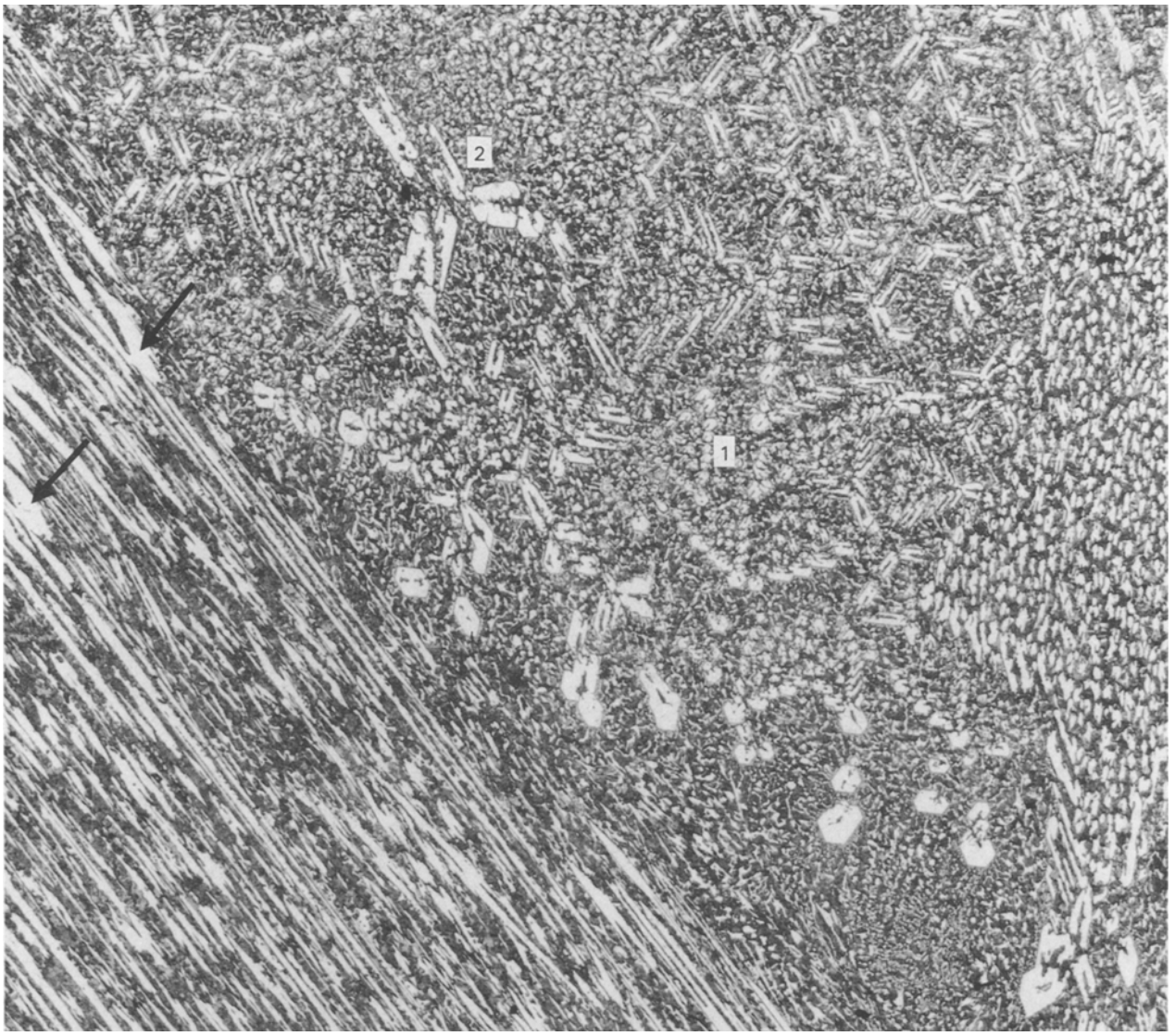


*Figure 2* Micrograph of hyper-eutectic sample, 20 wt % Cr and 4 wt % C, undercooled > 100 K below the $M_7C_3$ liquidus. The arrows show joining between the carbide rods (white). In the top right-hand grain the plane of section is transverse to the rod axis. $M_7C_3$ rods aligned in equilateral arrays are marked 1, while 2 shows carbides with an included angle of approximately 120°.

and 3 wt % C sample undercooled > 100 K below both the austenite liquidus and the eutectic temperatures is shown in Fig. 3. There was a boundary concave towards the left between the eutectic grain on the left where the plane of section was approximately parallel to the $M_7C_3$ eutectic carbides, and a grain on the right where the plane of section was transverse to the carbide rods. Note that the diameter of the carbide rods was much smaller than in the hyper-eutectic sample of Fig. 2. Again, the carbide rods were joined as shown by the arrows. These fine carbide rods were consistent with a much higher growth rate as evidenced by substantial recalescence [10].

The carbide rods within a eutectic grain were polycrystalline as shown by Laue photographs [10] and EBSD [11]. Fig. 4 shows a typical area of an undercooled hypo-eutectic alloy similar to that in Fig. 3 but at a higher magnification. The microtexture of the eutectic carbides of Fig. 4 is shown in the inverse pole figure of Fig. 5. Unexpectedly, there was no texture near [0 0 0 1] but a weak texture close to [1 0 $\bar{1}$ 1]. No twins were observed within the individual carbide rods. The reason for this texture will be investigated by analytical electron microscopy of thin foils of the joints of the carbides. It may represent branching by nucleation on active growth sites on the sides of the carbide rods as occurs in the growth of silicon carbide rods in the vapour–liquid–solid process [14].

## 3.2. Application of microstructural data from undercooled specimens

### *3.2.1. Carbide morphology in hardfacing weld deposits*

The fine eutectic of Fig. 1 is illustrated in Fig. 6, where the joints between adjacent rods are shown by arrows. An indication of the growth process of the fine eutectic of Fig. 6 is shown by Figs 7 and 8. In Fig. 7, the SEM micrograph shows the distribution of eutectic $M_7C_3$ carbides after the matrix of a conventionally polished specimen was removed by acid etching. Note that the carbides appeared to have grown in a colony or cellular mode from the bottom left to top right with an elongated cell tip similar to that reported by Matsu-

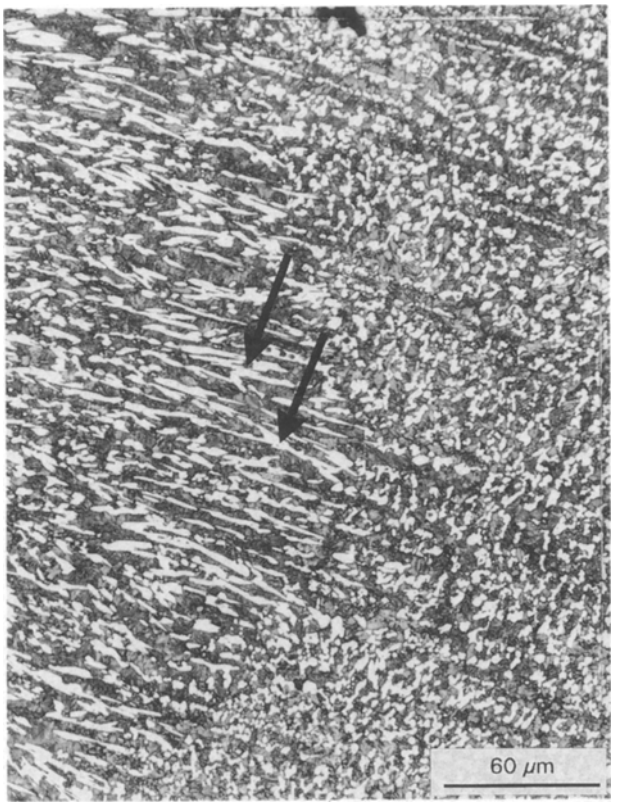


*Figure 3* Microstructure of hypo-eutectic sample, 20 wt % Cr and 3 wt % C, undercooled > 100 K below the eutectic temperature. The arrows show joining of the eutectic $M_7C_3$ carbide rods (white).


*Figure 4* Typical area of sample in undercooled hypo-eutectic alloy similar to that of Fig. 3 subjected to EBSD.

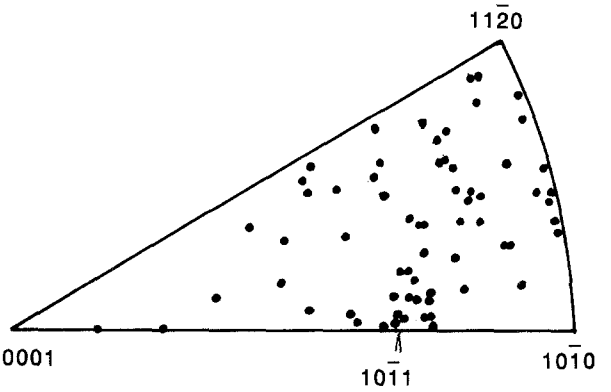


*Figure 5* Inverse pole figure for the normal to the specimen surface of the sample in Fig. 4 (i.e. the direction of the carbide rod axes if the specimen was polished perpendicular to the rods). There was a texture, near [1 0 $\bar{1}$ 1] predominantly and not near to [0 0 0 1].

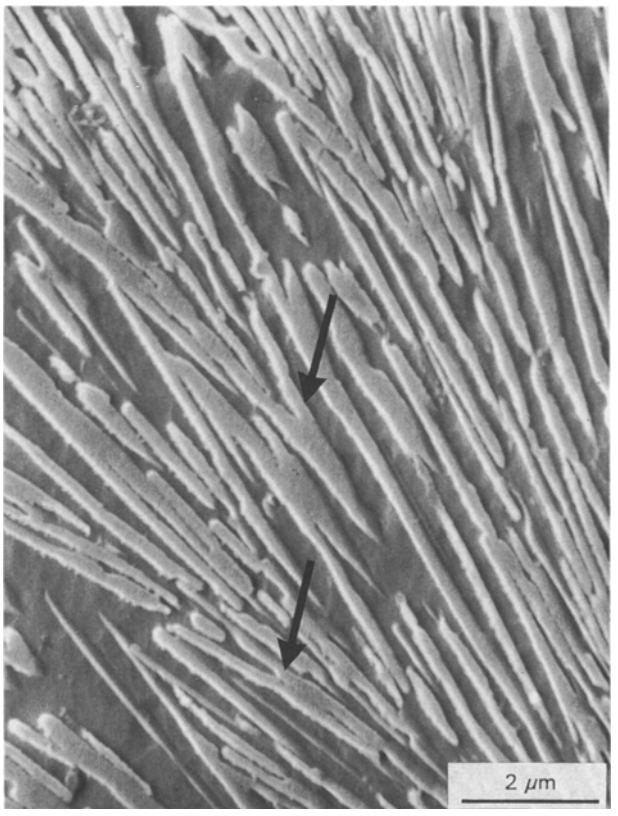


*Figure 6* Micrograph of the fine eutectic of $M_7C_3$ carbide plus austenite similar to that shown in Fig. 1. Joints in the eutectic carbides are arrowed.

bara and co-workers [15, 16] for unidirectionally solidified Fe–Cr–C alloys. In agreement with this suggested mode of growth, Fig. 8 shows that the carbides (arrowed) at the periphery of the tip were coarser than those near the centre. Note the hole in the centre of the carbide rods which resulted from dissolution of the matrix core during deep etching. The fact that the carbides retained the spatial distribution of an elongated cell-tip colony growth after deep etching provided further evidence that the eutectic carbides were joined together.

It is now possible to suggest how the microstructure develops in Fe–Cr–C hardfacing weld deposits laid


*Figure 7* SEM micrograph of fine eutectic $M_7C_3$ carbides after deep etching to remove the matrix. Cellular growth from bottom left to top right is apparent with elongated cell tips.

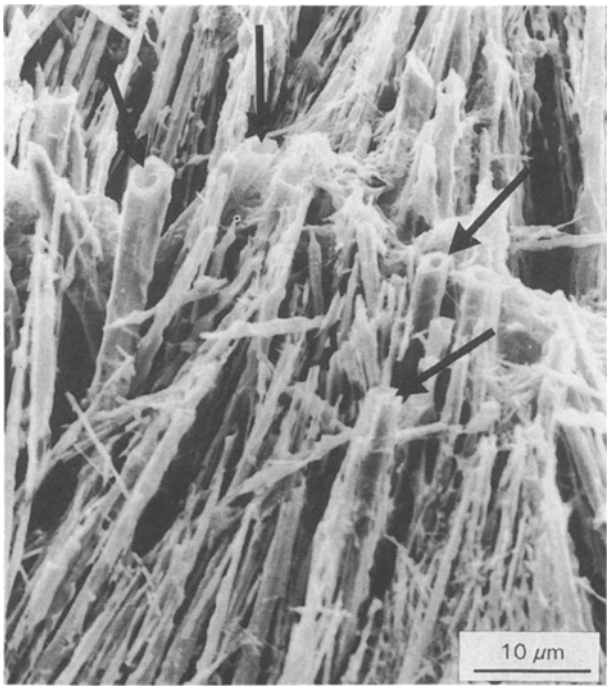


*Figure 8* SEM micrograph of eutectic carbides near end of cell tip showing coarser carbides (arrows) around the periphery of the tip. Note holes in carbides from dissolution of matrix core by deep etching.

down with the manual metal arc process. According to Svensson *et al.* [17], the cooling rate of the weld deposit in this process is $\sim 25\ K\ s^{-1}$. At such a fast cooling rate, undercooling before nucleation and growth occurs, as evidenced by the similarity of the welded microstructure and those of deliberately undercooled specimens. In addition to the growth of the carbide arrays from an undercooled weld deposit, it is probable that the fine eutectic of Figs 6–8 also grew from an undercooled weld deposit. Thus, the carbide in both cases would be branched with the same textures as those for the undercooled samples shown in Figs 2 and 3. It follows that if a crack was initiated as the result of stresses produced by dimensional changes during cooling the continuity of the carbide would facilitate crack propagation.

### 3.2.2. Effect of silicon additions on morphology of $M_7C_3$ carbides in Fe–Cr–C–Si alloys

Fig. 9a–c shows the top surfaces of solidified 50 g ingots of nominal 0 wt % Si (S1), 3.6 wt % Si (S2) and 6.9 wt % Si (S3), respectively, prepared from pure metals. The nominal and actual compositions are shown in Table I. The suffix (N) indicates the nominal composition while (P) shows the analysis of an alloy prepared with pure materials. S2(C) and S3(C) are the analyses for alloys of nominal compositions S2 and S3, respectively, using commercial purity starting materials. The nominal compositions are those investigated by Atamert and Bhadeshia [8, 9] to simultate the effect of silicon in Fe–Cr–C–Si hardfacing alloys.

Inspection of Fig. 9 revealed that growth from nucleation centres on the top surface occurred in all three alloys with fewer nucleation centres for the 3.6 wt % Si alloy (S2) and the 6.9 wt % Si alloy (S3). Similarly, in Fig. 10 it can be seen that growth proceeded from nucleation centres on the top surfaces when the ingots were prepared from commercially pure starting materials. It appeared that silicon had a large effect on reducing the number of nucleation centres but that the purity of the starting materials had only a minimal effect.

The microstructures of all five ingots shown in Figs 9 and 10 were similar. The microstructures of two specimens with similar compositions but made from starting materials of different purities are shown in Fig. 11. The nominal silicon content for the specimens of Fig. 11 was 6.9 wt % Si. In both micrographs a boundary between a grain on the right, where the plane of polish was transverse to the carbide rods, and a grain on the left, where the plane of polish was parallel to the carbide rods, could be observed. Note

TABLE I Chemical compositions of Fe–Cr–C–Si alloys

| No. | C | Cr | Si | Mn | Al | S | P |
|---|---|---|---|---|---|---|---|
| S1(N) | 3.90 | 33.6 | – | – | – | – | – |
| S2(N) | 4.48 | 34.4 | 3.6 | – | – | – | – |
| S2(C) | 4.11 | 34.0 | 3.57 | 0.22 | 0.01 | 0.01 | 0.01 |
| S3(N) | 3.60 | 31.2 | 6.90 | – | – | – | – |
| S3(P) | 3.50 | 29.9 | 7.03 | < 0.05 | < 0.01 | < 0.01 | < 0.01 |
| S3(C) | 3.21 | 31.6 | 7.10 | 0.29 | 0.06 | 0.01 | 0.01 |

(N), nominal; (P), alloy prepared using pure materials; (C), alloys prepared using commercial materials; C and S by combustion, other elements by optical emission spectroscopy.

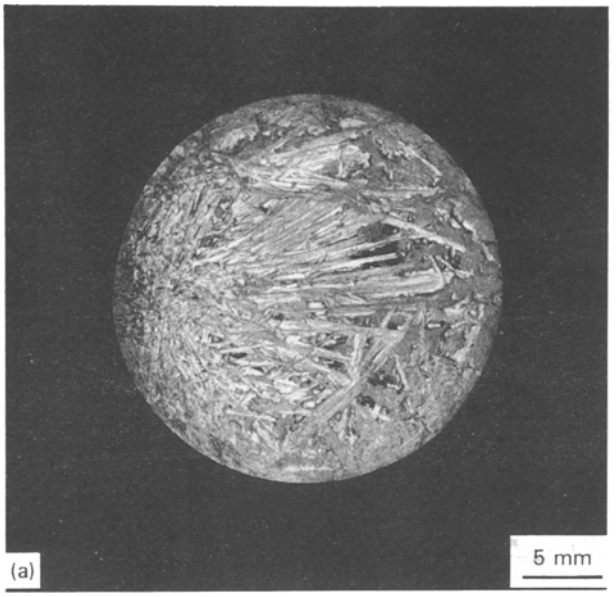


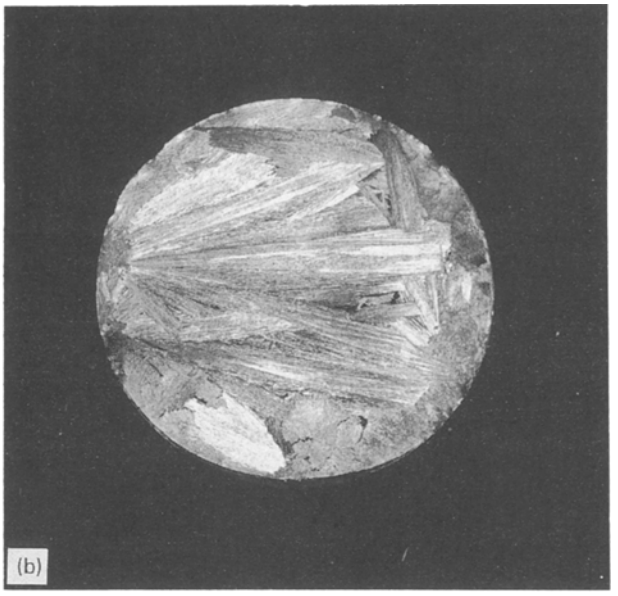


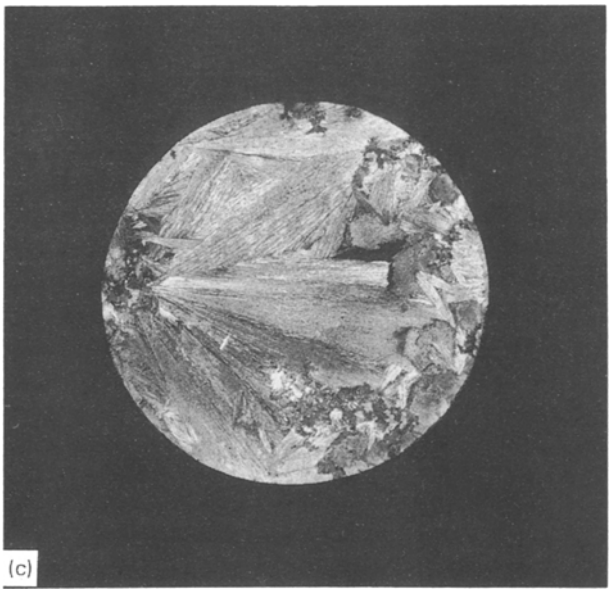


*Figure 9* Macrographs of the top surfaces of alloys S1 (a), S2 (b) and S3 (c). Starting with pure materials the silicon content varied from zero (S1) to 3.6 wt % (S2) to 6.9 wt % (S3). Note growth from nucleation centres on top surfaces.

that in the transverse plane the carbide rods tended to be arranged with three-fold rotational symmetry. This is especially apparent in Fig. 11a where the carbide rods were arranged in equilateral triangles (arrowed).

In these ingots the appearance of the $M_7C_3$ carbides in the plane of polish transverse to the axis of the carbide rods was similar to that shown in Fig. 2 for an undercooled hyper-eutectic alloy and indicated that undercooling occurred prior to solidification. Since silicon was more effective in eliminating nucleation centres (Fig. 10) than the purity of the starting materials (Fig. 9a) silicon appeared to be effective in producing undercooling, in agreement with a previous

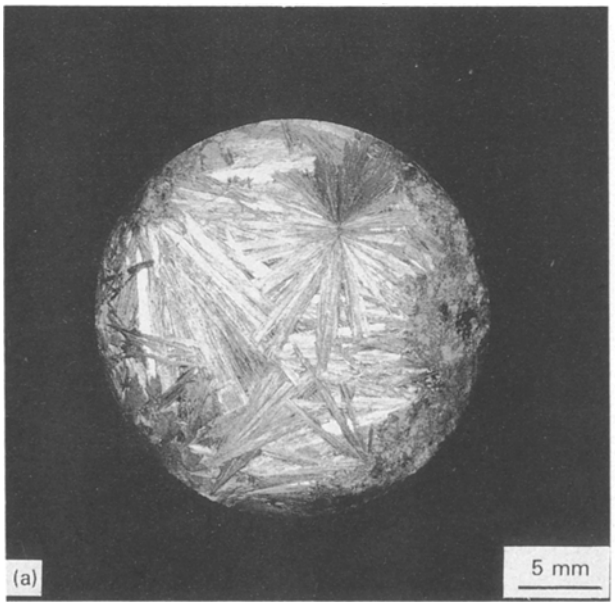


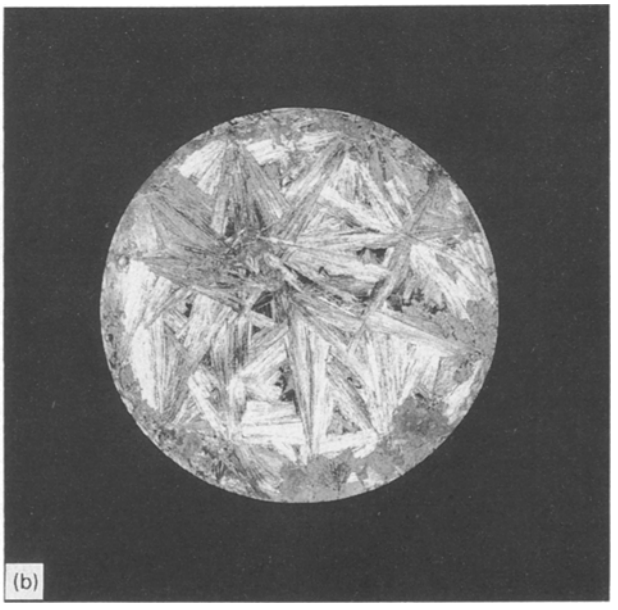


*Figure 10* Macrographs of the top surfaces of alloys S2 (a) and S3 (b) made from commercially pure materials. The silicon content varied from 3.57 (a) to 7.1 wt % (b).

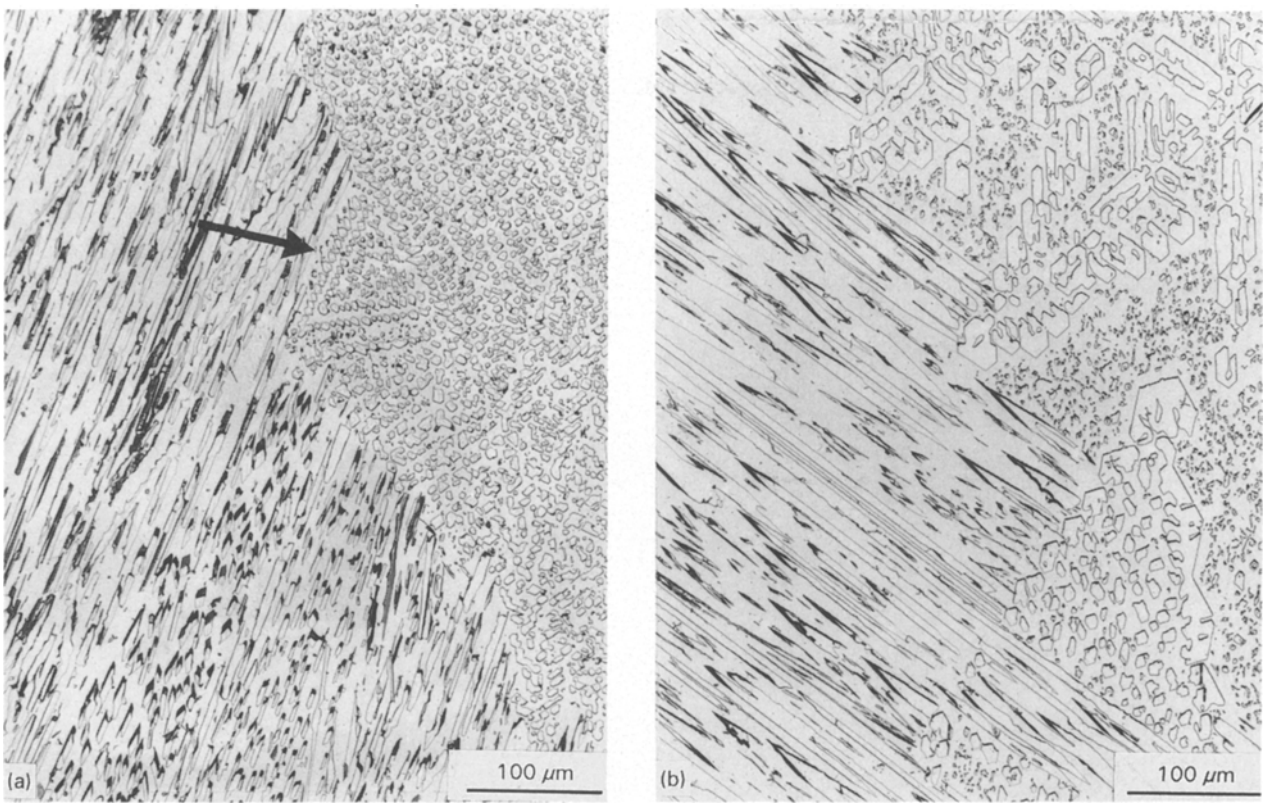


*Figure 11* Micrographs of S3(P) in (a) and S3(C) in (b). There are two grains in each micrograph. In (a) an equilateral array of carbides is indicated by the arrow.

report [18]. The appearance of the carbides in the transverse plane of polish was changed from the expected microstructure of a hyper-eutectic alloy. The normal microstructure of a hyper-eutectic alloy consists of large randomly nucleated and oriented primary $M_7C_3$ rods in a eutectic matrix of fine interconnected $M_7C_3$ rods and austenite. Thus, the carbides on the right-hand side of Fig. 11a and b could be interpreted as a more equiaxed morphology if not examined in a SEM after deep etching to remove the matrix. This is the likely explanation for the conclusion by Atamert and Bhadeshia [8, 9] that the addition of silicon produced a change in morphology of the $M_7C_3$ carbides towards a more equiaxed shape, as these authors relied solely on optical metallography.

## 4. Conclusions

1. In an undercooled hyper-eutectic Fe–Cr–C alloy slow growth from the melt produced $M_7C_3$ carbide rods that were coarse, monocrystalline and joined together with a [0001] growth texture.
2. In an undercooled hypo-eutectic Fe–Cr–C alloy, rapid growth from the melt resulted in a eutectic $M_7C_3$ carbide morphology consisting of fine rods joined together with a weak $[10\bar{1}1]$ texture. There were no twins in the individual rods and the branching was inconsistent with a simple twinning mechanism.
3. The microstructure of the first and second layers of a multi-layered Fe–Cr–C hardfacing weld deposit applied by the manual metal arc process could be explained in terms of undercooling of hypo- to hyper-eutectic compositions.
4. The morphology of the $M_7C_3$ carbides in compositions varying from hypo- to hyper-eutectic is continuous.
5. The effect of silicon on hyper-eutectic Fe–Cr–C–Si alloys with silicon up to 7 wt % was to produce undercooling and therefore a change in the morphology of the $M_7C_3$ carbides from that in the normal microstructure of a hyper-eutectic alloy to that characteristic of an undercooled alloy. This was not a change to a more equiaxed morphology and the carbides were still continuous.

## Acknowledgements

The authors thank Mr Guenter Herfurth for optical metallography, Mr Peter Lloyd for SEM and Mr Trevor Kenyon for macrophotography.

## References

1. D. E. DIESBURG and F. BORIK, Symposium "Materials for the Mining Industry" ed. R. G. Barr, 1974, Climax Molybdenum, Vail, USA, p. 15.
2. ASTM A532-87, Standard Specification for Abrasion-Resistant Cast Irons.
3. "Metals handbook", 9th Edn, Vol. 6 (Welding, Brazing, and Soldering, ASM OH, 1983) p. 779.
4. *ibid.* p.776.
5. "Fractographic atlas of steel weldments" (Japan Welding Society, 1982) p. 234.
6. G. L. F. POWELL, Australian Welding Research 6 (1979) 16.
7. G. L. F. POWELL, *J. Mater. Sci. Lett.* **10** (1991) 745.
8. S. ATAMERT and H. K. D. H. BHADESHIA, "Proc. of heat treatment '87" (Institute of Metals, London, 1988) p. 39.
9. S. ATAMERT and H. K. D. H. BHADESHIA, "Recent trends in welding science and technology TWR '89", edited by S. A.

David and J. M. Vitek (ASM International, Materials Park, USA, 1990) p. 273.
10. G. L. F. POWELL, *Mater. Trans. JIM* **31** (1990) 110.
11. V. RANDLE and G. L. F. POWELL, *J. Mater. Sci. Lett.* **12** (1993) 779.
12. G. L. F. POWELL and L. S. HEARD, *Trans. Jpn Inst. Metals* **22** (1981) 543.
13. R. ELLIOTT, "Eutectic solidification processing" (Butterworths, London, 1983) p. 85.
14. J. V. MILEWSKI, F. D. GAC, J. J. PETROVIC and S. R. SKRAGGS, *J. Mater. Sci.* **20** (1985) 1160.
15. Y. MATSUBARA, K. OGI and K. MATSUDA, *AFS Trans.* **1989** (1981) 183.
16. K. OGI, Y. MATSUBARA and K. MATSUDA, *ibid.*, 197.
17. L. E. SVENSSON, B. GRETOFT, B. ULANDER and H. K. D. H. BHADESHIA, *J. Mater. Sci.* **21** (1986) 1015.
18. G. LAIRD and G. L. F. POWELL, *Metall. Trans.* **24A** (1993) 981.

*Received 17 December 1992*
*and accepted 9 February 1994*